Superamphiphobic, light-trapping $FeSe_2$ particles with a micro-nano hierarchical structure obtained by an improved solvothermal method*

Yu Jing(郁 菁), Wang Hui-Jie(王会杰), Shao Wei-Jia(邵伟佳), and Xu Xiao-Liang(许小亮)†

Department of Physics, University of Science and Technology of China, Hefei 230026, *China*

(Received 31 May 2013; revised manuscript received 14 August 2013; published 2 December 2013)

Wettability and the light-trapping effect of $FeSe_2$ particles with a micro-nano hierarchical structure have been investigated. Particles are synthesized by an improved solvothermal method, wherein hexadecyl trimethyl ammonium bromide (CTAB) is employed as a surfactant. After modifying the particles with heptadecafluorodecyltrimethoxy-silane (HTMS), we find that the water contact angle (WCA) of the $FeSe_2$ particles increases by 6.1° and the water sliding angle (WSA) decreases by 2.5° respectively, and the diffuse reflectivity decreases 29.4% compared with similar $FeSe_2$ particles synthesized by the conventional method. The growth process of the particles is analyzed and a growth scenario is given. Upon altering the PH values of the water, we observe that the superhydrophobic property is maintained quite consistently across a wide PH range of 1–14. Moreover, the modified particles were also found to be superoleophobic. To the best of our knowledge, there is no systematic research on the wettability of $FeSe_2$ particles, so our research provides a reference for other researchers.

Keywords: $FeSe_2$, superhydrophobic, micro-nano hierarchical structure, light-trapping

PACS: 68.08.Bc, 68.08.–p, 81.07.Bc **DOI:** 10.1088/1674-1056/23/1/016803

1. Introduction

In recent years, transition-metal chalcogenides have increasingly been a hot topic among researchers due to their tunable optical, electrical, and magnetic properties.[1–6] Among these substances, $FeSe_2$ is of particular interest due to its applications in solar cells. It possesses narrow band-gap energy ($E_g = 1.0$ eV) and a high optical absorption coefficient, which together make $FeSe_2$ an alternative to Si.[6–9] Various methods of synthesizing $FeSe_2$ particles have been proposed by researchers in the last decade, including soft selenization of iron films, low-pressure metal organic chemical vapor deposition, hydrothermal synthesis, solvothermal synthesis, photochemical deposition, etc.[6,7,9–13] Different synthetic methods endow $FeSe_2$ with various morphologies and sizes, which give rise to diverse useful physical properties. Although researchers have demonstrated lots of interesting physical characteristics of $FeSe_2$, many of its properties have yet to be studied. As a result, researching some fundamental properties of $FeSe_2$ is still necessary for our further investigation.

Wettability is a very valuable physical property for surface materials, with many potential applications, both in our daily life and in industrial production. Materials with a water contact angle larger than 150° and a sliding angle less than 10° are usually regarded as superhydrophobic materials.[14] Previous studies have shown that micro-nano hierarchical structures and low surface energy both have important influence on superhydrophobic performance.[15,16] In accord with these fundamentals, there are two basic strategies for obtaining superhydrophobic surfaces: (1) directly constructing micro-nano hierarchical structures of low-surface-energy materials;[17,18] (2) building micro-nano hierarchical structures of other materials and modifying them with low-surface-energy chemicals.[19–24] Generally, method (2) is popular among researchers due to many options of materials. Although $FeSe_2$ is a potential surface material, its wettability has not been systematically investigated to date. Due to the high surface energy of $FeSe_2$, method (2) is the only approach for us to make the $FeSe_2$ superhydrophobic.

Flower-like $FeSe_2$ particles synthesized by a solvothermal method have been reported by Luan's group.[6] They used oleylamine as the solvent, ferric oxide as the iron source, and selenium powder as the selenium iron. In view of the special morphology of this $FeSe_2$ material, we research its wettability and find it to be superhydrophobic after being modified with the HTMS. To acquire better superhydrophobic performance, we improve the synthesis method by adding a moderate amount of CTAB in the solution and obtain micro-nano hierarchical flower-like $FeSe_2$ particles that have more 'petals' than Luan's. These micro-nano hierarchical structures make the $FeSe_2$ particles more superhydrophobic, with the water contact angle (WCA) increased by 6.1° and the water sliding angle (WSA) decreased 2.5° repectively. To systematically investigate the wettability of these two $FeSe_2$ particles, we not

*Project supported by the Natural Science Foundation of Anhui Province, China (Grant No. 12010202035) and the National Natural Science Foundation of China (Grant No. 51272246).

†Corresponding author. E-mail: xlxu@ustc.edu.cn

© 2014 Chinese Physical Society and IOP Publishing Ltd

only study the superoleophobic properties of the particles, but also study effects of the water droplets' PH values on the superhydrophobic properties of the particles. We find that these $FeSe_2$ particles perform better in both respects. Lastly, we test the diffuse reflectivities of these two $FeSe_2$ particles and find that our improved particles also have lower reflectivity than the original particles. In one word, based on these results, we think our research will encourage others to investigate additional meaningful properties of such $FeSe_2$ particles.

2. Experimental

2.1. Materials

Selenium powder (Se, AR) was obtained from Shanghai Meixing Chemical Reagent Co., China; oleylamine (OLA, 70%) was obtained from Sigma-Aldrich (USA); and the heptadecafluorodecyltrimethoxy-silane (HTMS) was made by Dow Corning Co. (USA). Other reagents, including ferric oxide (Fe_2O_3, AR), hexadecyl trimethyl ammonium bromide (CTAB, AR), absolute alcohol (AR), hexahydrobenzene (AR), and toluene (AR) were all purchased from Sinopharm Chemical Reagent Co., Ltd. Moreover, all the above chemicals were used without further purification. Cover glasses (22 mm $\times$ 22 mm $\times$ 0.15 mm) were purchased from Jiangsu Feizhou Plastic Products Co., China.

2.2. Synthesis of $FeSe_2$ particles

Two solutions (experimental solution and contrasted solution) are needed in the synthesis. The contrasted solution was synthesized as follows: Se powder (0.67 mmol), Fe_2O_3 powder (0.083 mmol), and OLA (5 ml) were placed together in a flask (10 ml), then the mixture was stirred for 20 min to make the solution homogeneous. The experimental solution was substantially the same as the contrasted one, except that an ethanol solution of CTAB (1200 μl, 0.27 M) was put into the flask with 3 min of additional stirring. Then the two flasks were heated at 220 °C for 2 h. After the heat treatment, the flasks are cooled to room temperature naturally. The solutions were centrifuged at 8000 rpm for 5 min, after which the supernatant was discarded and the remaining precipitates were washed 5 times with a solution of alcohol/hexahydrobenzene (4/1 vol.). At last, these precipitates were dried overnight in a vacuum and preserved for further characterization. For simplicity, the precipitates obtained from the experimental solution will be called sample 1, and those obtained from the contrasted solution will be called sample 2. A schematic of the synthesis of different $FeSe_2$ particles is shown in Fig. 1.

2.3. Modification of the particles

One third of sample 1 and sample 2 were mixed with absolute alcohol (500 μl) respectively to form rheumy 'coatings', which were then coated on two cover glasses, respectively. Toluene (3 ml) and HTMS (150 μl) were added into a beaker (10 ml), followed by an ultrasonic treatment. The two glasses and the beaker were put into a sealed box and were heated in the drying oven for 3.5 h at 85 °C. After the heat treatment, the box was opened in a draught cabinet and the cover glasses were allowed to cool to ambient temperature naturally.

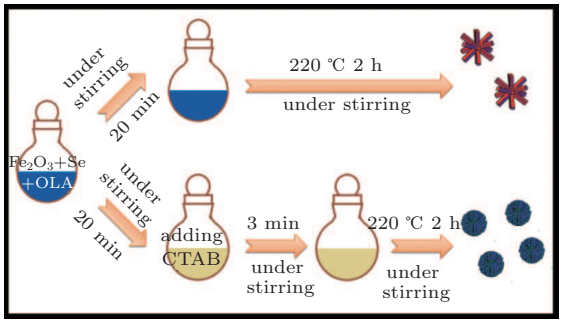


Fig. 1. (color online) Schematic of the synthesis of different $FeSe_2$ particles.

2.4. Characterization

X-ray diffractive patterns (2θ ranges from 20° to 70°) obtained from an X-ray diffractometer (TTR-III), using Cu-Kα radiation ($\lambda = 0.154$ nm), were utilized to research the crystallization, purity, and phase of the particles. Morphological structures of the $FeSe_2$ particles were studied by scanning electron microscopy (SEM) images, which were obtained on a field emission scanning electron microscope (JSM-6700F). To analyze the nanostructure and the crystallization direction of the $FeSe_2$ 'petals' transmission electron microscopy (TEM) images, high-resolution transmission electron microscopy (HRTEM) images and selected area electron diffraction (SAED) images were obtained by a HRTEM system (JEM-2011). Static contact angle (CA) and sliding angle (SA) are the key characterizations for the superhydrophobic and superoleophobic properties of any material. They were measured by a Contact Angle Tester SL200B (Solon Tech Co., Ltd. Shanghai) and its related software (CAST 2.0). The water (oil) droplets we used were all 4.5 (2.0) μl and all the values of CAs and SAs given in this paper are averages obtained by measuring five times at different points of the same samples. Light-trapping effects of the particles were tested by a SolidSpec-3700 UV-VIS-NIR spectrophotometer (SHIMADZU) in the wavelength range from 300 nm to 1200 nm.

3. Results and discussion

The crystallization, purity, and phase are studied by powder X-ray diffraction. Figure 2 shows the XRD patterns of the $FeSe_2$ particles in the 2θ range from 20° to 70°. The particles prove to be orthorhombic iron selenide with all peaks in the patterns corresponding well with the standard diffraction peaks (PDF#65-1455) and no impure peaks appearing in

the patterns. Moreover, the peaks are all sharp and narrow, which suggests high crystallization of the particles. Cell parameters of the particles are calculated as follows. Sample 1: $a = 4.801$ Å, $b = 5.781$ Å, $c = 3.578$ Å, (2) sample 2: $a = 4.798$ Å, $b = 5.779$ Å, $c = 3.579$ Å. These parameters are slightly different from the standard values ($a = 4.804$ Å, $b = 5.784$ Å, $c = 3.586$ Å), probably due to the microscopic stress inherent in the flower-like structures.

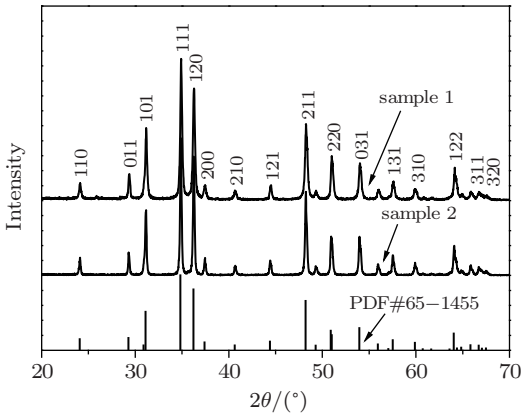


Fig. 2. XRD patterns of the two samples.

SEM images of the particles are shown in Fig. 3. Figures 3(a) and 3(c) are images of sample 1 and sample 2, respectively; figures 3(b) and 3(d) are corresponding magnified images of Figs. 3(a) and 3(c). From Figs. 3(c) and 3(d), it is clear that the size of sample 2 is 2.5–4.5 μm, and the length and width of the 'petals' are 310–1500 nm and 100–400 nm, respectively. Compared with sample 2, examples of sample 1 are more regular and closer to sphere with diameter of 1.3–2.0 μm, average 'petal' length of 283 nm, and average 'petal' width of 60 nm. Moreover, the 'petals' of sample 1 particles are denser than those of sample 2. To account for these results, we propose this growth scenario: at the beginning of the experiment, $FeSe_2$ seed crystals are the original form of the particles in the solution; these seed crystals undergo two synchronous processes: (i) self growth of the seed crystals; (ii) polar assembly of different seed crystals. Process (i) makes the seed crystals grow to rod-like particles and process (ii) makes these rod-like particles form flower-like structures. For certain total quantities of the reactive materials, 'petals' of particles become long, wide, and low-density in condition that the effect of process (i) is stronger than that of process (ii). Otherwise, 'petals' become short, narrow, and high-density. For a growing environment without CTAB, process (i) is dominant, as can be observed in Figs. 3(c) and 3(d). After the CTAB is added into the solution, seed crystals adsorb some Br^- ions on their surfaces, which reduces both the growth of the seed crystals and the polar assembly rate of different seed crystals. From Figs. 3(b) and 3(d), it is reasonable to believe that the growth rate of the seed crystals is slower than the polar assembly of different seed crystals. Thus, CTAB makes process (ii) play the leading role in the reaction. On account of this effect, different morphological structures of $FeSe_2$ particles were observed in our experiment.

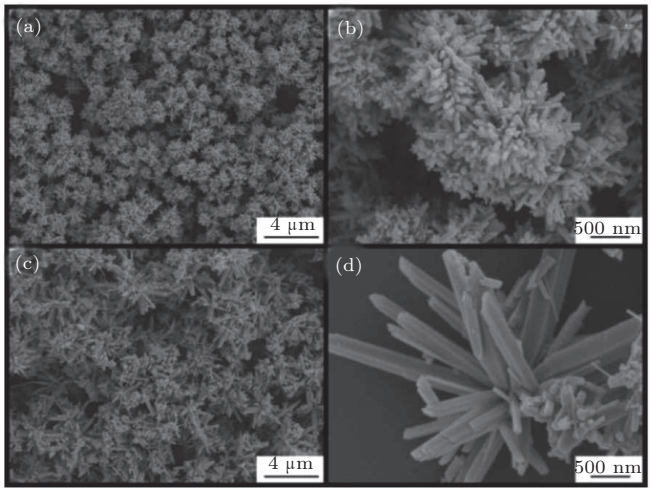


Fig. 3. SEM images of flower-like $FeSe_2$ particles: (a) sample 1, (c) sample 2, (b) and (d) corresponding magnified images of (a) and (c), respectively.

A TEM image, an HRTEM image, and an SAED pattern of the $FeSe_2$ 'petals' are all shown in Fig. 4. The fringes in Fig. 4(b) and the diffraction points in the inset reveal that the rod-like 'petals' are well-crystallization single crystals. There are two kinds of fringes in Fig. 4(b), which are mutually perpendicular. The plane intervals of different fringes are 3.70±0.05 Å and 3.60±0.04 Å, respectively. By comparing these measurements with the values provided by the Powder Diffraction File (PDF#65-1455), it is reasonable to believe that the two fringes correspond to the (110) lattice plane (3.69 Å) and the (001) lattice plane (3.58 Å), respectively. Moreover, we can also determine that the direction of the zone axis is $(\bar{1}10)$. By measuring the distances between different points in the insets, we obtain that $R_2/R_1 = 1.477$, $R_2/R_3 = 0.637$, $R_3/R_1 = 2.318$, $\theta_1 = 45.7 \pm 0.2°$, and $\theta_2 = 18.3 \pm 0.2°$, where R_1, R_2, and R_3 are the distances from the origin of the diffractive pattern to the nearest, second nearest, and third nearest diffractive points, respectively; $\theta_1(\theta_2)$ is the angle between line R_1 and line R_2 (line R_2 and line R_3). Therefore, it is easy to confirm that the directions of R_1, R_2, and R_3 are (110), (111), and (221), respectively. It is worth noting that the standard values are $R_2/R_1 = 1.436$, $R_2/R_3 = 0.638$, $R_3/R_1 = 2.251$, $\theta_1 = 45.9°$, and $\theta_2 = 18.6°$. By use of these values obtained from the SAED pattern, the zone axis can be determined to be $(\bar{1}10)$, which agrees well with the results obtained by the HRTEM image. To sum up, these results are sufficient to prove that the rod-like 'petals' grow along the (110) direction and are well-crystallization single crystals.

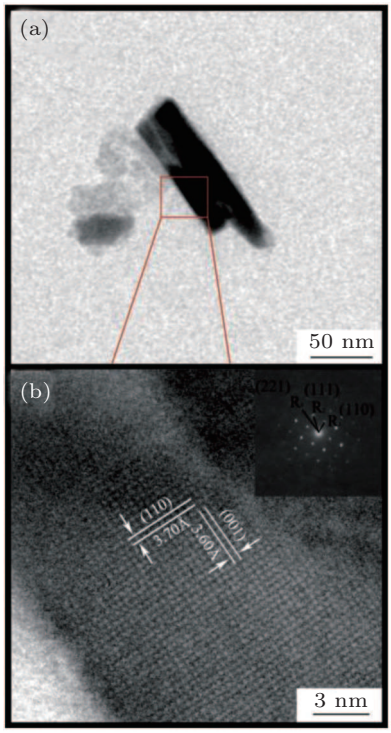


Fig. 4. (color online) (a) TEM image of the $FeSe_2$ 'petals'. (b) HRTEM image of the edge area of the $FeSe_2$ 'petals'. Inset in (b) is the SAED pattern of the $FeSe_2$ 'petals'.

The superhydrophobic and superoleophobic properties of the modified particles are researched in this paper. Water CA images and snapshot photographs of water droplets rolling off differently slanted surfaces are shown in Fig. 5. Oil CAs and SAs are exhibited in Table 1. Figures 5(a) and 5(b) tell us that sample 1 has a larger CA ($156.2 \pm 2.0°$) than sample 2 ($150.1 \pm 2.5°$), which suggests that the improved particles have better superhydrophobicity. According to the foregoing descriptions, the 'petals' of sample 1 are denser than those of sample 2 while also being shorter and narrower, so sample 1 possesses a micro-nano hierarchical structure in contrast with sample 2 which possesses a single micro-scale structure. This structural contrast accounts for sample 1 and sample 2 following different models from liquid contact theory: the Cassie model and the Wenzel model are suitable for describing the properties of sample 1 and sample 2, respectively, as shown in Fig. 6. The greatest difference between the two models is that, in a droplet's surface-contact area, in the Wenzel model, the liquid contacts the surface only, while in the Cassie model, the liquid contacts the surface partially and also contacts some air. Hence, a droplet in the Cassie model tends to retain a more spherical shape, which results in the improved $FeSe_2$ particles having a larger CA than the unimproved ones. Figures 5(b1–b4) and 5(a1–a4) show that the SAs of sample 1 and sample 2 are $2.5 \pm 1.0°$ and $5 \pm 0.8°$, respectively, which further proves that sample 1 is more superhydrophobic than sample 2. These low SAs guarantee that the samples have an excellent "self-cleaning" function, which plays an important role in their potential applications in surface materials. The oil CAs and SAs of the samples are given in Table 1. Three kinds of oil (ethylene glycol, diiodomethane, formamide) were used to prove the universality of the particles' superoleophobic property. From Table 1, it is found that both the two samples are superoleophobic except that the diiodomethane CA of sample 2 is $149.2 \pm 4.0°$. For the same oil, the superoleophobic property of sample 1 is commonly better than that of sample 2, which is reflected in both larger CAs and lower SAs.

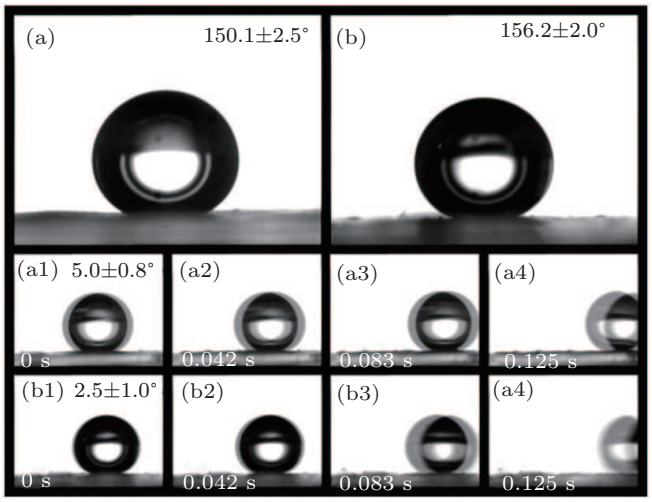


Fig. 5. (a) WCA image of sample 2. (b) WCA image of sample 1. (a1)–(a4) and (b1)–(b4) Snapshot photographs of water droplets rolling off the surfaces of sample 2 and sample 1, respectively.

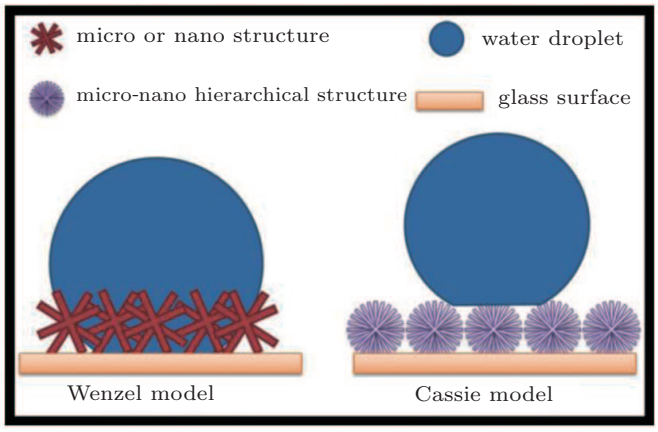


Fig. 6. (color online) Schematic of Wenzel and Cassie models.

Table 1. Oil CAs and SAs of the two samples.

		ethylene glycol	diiodomethane	formamide
CA/(°)	Sample 1	155.0±3.0	150.2±2.8	152.4±3.5
	Sample 2	150.2±3.2	149.2±4.0	150.0±3.8
SA/(°)	Sample 1	7.2±1.2	3.0±1.3	3.0±0.8
	Sample 2	8.2±1.1	3.5±1.5	4.0±1.0

To explore the wettability of the samples further, the effect of PH on water CAs and water SAs of samples is studied, as shown in Fig. 7. Figures 7(a) and 7(b) correspond to sample 1 and sample 2, respectively. In the two figures, it is clear that both sample 1 and sample 2 remain superhydrophobic in a wide PH range from 1 to 14 with only small fluctuations.

It is also clear that the superiority of sample 1 to sample 2 with regard to wettability is maintained in either an alkaline environment or an acidic environment. This wide-PH superhydrophobicity endows the $FeSe_2$ particles with specific anticorrosive functions, which can protect them well in various harsh environments.

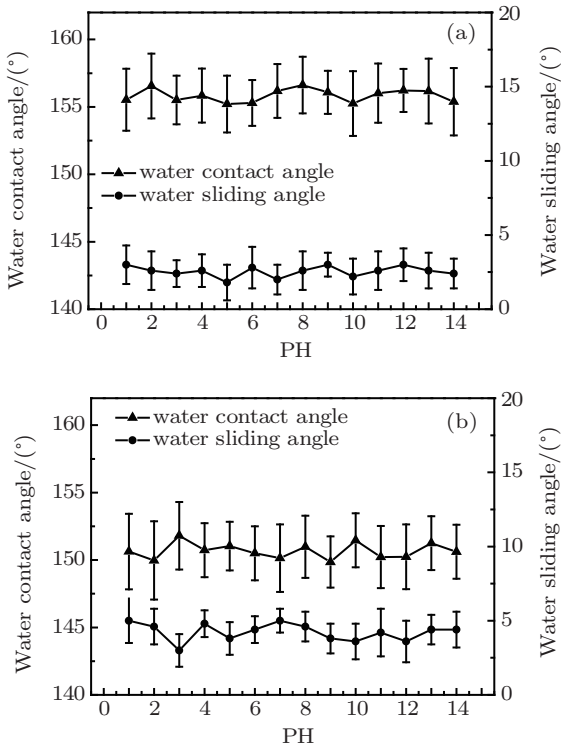


Fig. 7. Relationship between PH value and CA or SA: (a) sample 1, (b) sample 2.

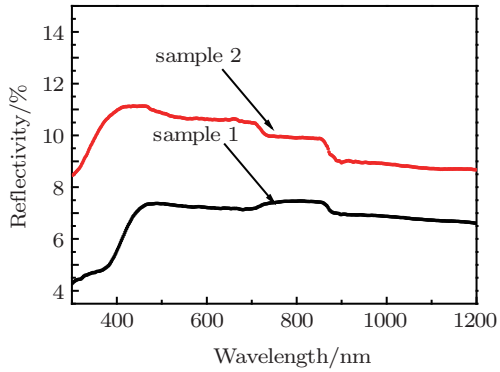


Fig. 8. (color online) Diffuse reflective spectra of the two samples.

According to all the results we obtain, it is reasonable to believe that our method significantly improves the wettability of $FeSe_2$ with respect to both superhydrophobicity and superoleophobicity.

In consideration of the applications of $FeSe_2$ in solar cells, an optical property of the samples is studied in this paper. Figure 8 shows the diffuse reflectivities of the two kinds of $FeSe_2$ particles. The reflectivity of sample 1 (average 6.96%) is always lower than that of sample 2 (average 9.86%) in the whole wavelength range (300–1200 nm), which can be ascribed to its unique micro-nano hierarchical structure. This micro-nano hierarchical structure can scatter incident light repeatedly between particles, increasing the effective scattering path length. Although a micro-scale structure can also bring about this phenomenon, the low density of microstructured 'petals' limits the effect, so they cannot extend the path length as far as the micro-nano structure can. Low reflectivity guarantees sufficient light absorption by $FeSe_2$ and makes our samples competitive in converting solar energy.

4. Conclusion

In summary, we research the superamphiphobicity and the light-trapping effect of flower-like $FeSe_2$ particles, and significantly improve both properties by altering the structure of the particles from a micro-scale structure to a micro-nano hierarchical structure with the help of CATB. An account of the mechanism of CTAB's influence is also made. We think this work will help others to understand the superamphiphobicity and light-trapping effect of these $FeSe_2$ particles and encourage them to investigate other meaningful fundamental properties of such $FeSe_2$ particles.

References

[1] Akhtar M, Akhtar J, Malik M A, Tuna F, Helliwell M and O'Brien P 2012 *J. Mater. Chem.* **22** 14970
[2] Park J, An K J, Hwang Y S, Park J G, Noh H J, Kim J Y, Park J H, Hwang N M and Hyeon T 2004 *Nat. Mater.* **3** 891
[3] Thanikilkarasan S, Mahalingam T, Sundaram K, Kathalingam A, Kim Y D and Kim T 2009 *Vacuum* **83** 1066
[4] Kathalingam A, Mahalingam T and Sanjeeviraja C 2007 *Mater. Chem. Phys.* **106** 215
[5] Tang K B, Qian Y T, Zeng J H and Yang X G 2003 *Adv. Mater.* **15** 448
[6] Yuan B X, Luan W L and Tu S T 2012 *Dalton T* **41** 772
[7] Xu J, Jang K, Lee J, Kim H J, Jeong J, Park J G and Son S U 2011 *Cryst. Growth Des.* **11** 2707
[8] Kwon H J, Thanikaikarasan S, Mahalingam T, Park K H, Sanjeeviraja C and Kim Y D 2008 *J. Mater. Sci.-Mater. Electron.* **19** 1086
[9] Mahalingam T, Thanikaikarasan S, Chandramohan R, Raja M, Sanjeeviraja C, Kim J H and Kim Y D 2007 *Mater. Chem. Phys.* **106** 369
[10] Ouertani B, Ouerfelli J, Saadoun M, Zribi M, Ben Rabha M, Bessais B and Ezzaouia H 2006 *Thin Solid Films* **511** 457
[11] Liu A P, Chen X Y, Zhang Z J, Jiang Y and Shi C W 2006 *Solid State Commun.* **138** 538
[12] Hamdadou N, Khelil A, Morsli M and Bernade J C 2005 *Vacuum* **77** 151
[13] Yang J, Cheng G H, Zeng J H, Yu S H, Liu X M and Qian Y T 2001 *Chem. Mater.* **13** 848
[14] Liu K S and Jiang L 2011 *Nanoscale* **3** 825
[15] Ming W, Wu D, van Benthem R and de With G 2005 *Nano Lett.* **5** 2298
[16] Nakajima A, Hashimoto K, Watanabe T, Takai K, Yamauchi G and Fujishima A 2000 *Langmuir* **16** 7044
[17] Zhang Y, Wei S, Liu F, Du Y, Liu S, Ji Y, Yokoi T, Tatsumi T and Xiao F S 2009 *Nano Today* **4** 135
[18] Nystrom D, Lindqvist J, Ostmark E, Hult A and Malmstrom E 2006 *Chem. Commun.* 3594
[19] Gong M G, Liu Y Y and Xu X L 2010 *Chin. Phys. B* **19** 106801
[20] Gong M G, Xu X L, Yang Z, Liu Y S and Liu L 2010 *Chin. Phys. B* **19** 056701
[21] Ma K, Li H, Zhang H, Xu X L, Gong M G and Yang Z 2009 *Chin. Phys. B* **18** 1942
[22] Yang Z, Wu Y Z, Ye Y F, Gong M G and Xu X L 2012 *Chin. Phys. B* **21** 126801
[23] Yang Z, Xu X L, Gong M G, Liu L and Liu Y S 2010 *Chin. Phys. B* **19** 126103
[24] Gong M G, Xu X L, Yang Z, Liu Y Y, Lü H F and Lü L 2009 *Nanotechnology* **20** 165602